JACS
JOURNAL OF THE AMERICAN CHEMICAL SOCIETY

ARTICLE

pubs.acs.org/JACS

Selective Catalytic Reduction at Quasi-Perfect Pt(100) Domains: A Universal Low-Temperature Pathway from Nitrite to N_2

Matteo Duca,*[,†] Marta C. Figueiredo,[‡] Victor Climent,[‡] Paramaconi Rodriguez,[†] Juan M. Feliu,[‡] and Marc T. M. Koper*[,†]

[†]Leiden Institute of Chemistry, Leiden University, P.O. Box 9502, 2300 RA Leiden, The Netherlands

[‡]Instituto de Electroquímica, Universidad de Alicante, Apt. 99, E-Alicante, Spain

ABSTRACT: The highly selective conversion of nitrite to N_2 at a quasi-perfect Pt(100) electrode in alkaline media was investigated with a particular emphasis on its structure sensitivity and its mechanism. High-quality (100) terraces are required to optimize the catalytic activity and steer the selectivity to N_2: defects of any symmetry dramatically reduce the N_2 evolution at [(100) × (110)] and [(100) × (111)] surfaces. On the other hand, nitrite reduction proves to be an additional example of the unique intrinsic ability of (100) surfaces to catalyze reactions involving bond breaking and successive bond formation. In the present case, (100) is able to reduce nitrite to $NH_{2,ads}$, which in a certain potential window combines with NO_{ads} to give N_2 in a Langmuir−Hinshelwood reaction. Our findings are similar to those for other processes generating N_2, from bacterial anoxic ammonia oxidation ("anammox") to the high-temperature NO + NH_3 reaction at Pt(100) crystals under ultra-high-vacuum conditions, thus suggesting that the combination of these two nitrogen-containing species is a universal (low-temperature) pathway to N_2. The advantages of this pathway over other N_2-generating pathways are pointed out.

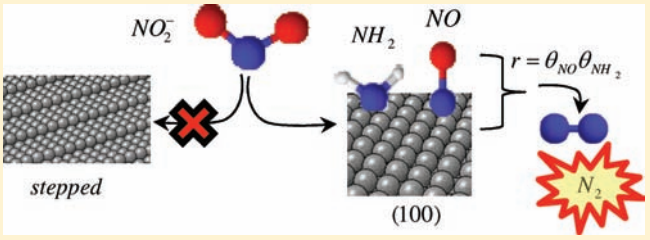

INTRODUCTION

The global imbalances in the nitrogen cycle have been investigated by several authoritative studies in the field of the environmental sciences,[1,2] which have shown that this issue poses a threat potentially more menacing than CO_2 accumulation. The extraction of atmospheric N_2 via combustion (to NO_x) or via the Haber−Bosch synthesis of NH_3 has led to an accumulation of nitrogen oxyanions in soils and groundwater due to acid deposition and consequent runoff (for atmospheric NO_x) or overuse of ammonium fertilizers, ultimately leading to the production of nitrate and nitrite by bacterial reactions. Therefore, the levels of nitrate and nitrite in ground- and wastewater must be kept under close scrutiny, and novel abatement methods, superior to the widespread but energy-intensive bacterial active-sludge treatment,[3−5] are urgently needed.

Electrochemical processes could ideally be used to treat nitrate-laden aqueous waste, provided that the activity is optimized and full selectivity to N_2 is achieved, thus creating a human-driven closed detour of the geochemical nitrogen cycle. Both requirements have spurred wide-ranging research[6] addressing potential nitrogen-containing pollutants such as NO, NO_2^-, and NO_3^-. In addition, the electrochemical reactivity of these simple molecules offers significant insight into fundamental mechanistic aspects of the redox features of the nitrogen cycle.[7] From this point of view, numerous studies[7] have highlighted the complex reaction pathways of the electrochemical reduction of NO_2^- [8−16] and NO_3^-,[17−22] with a potentially wide range of products. This lack of product selectivity has prompted an ongoing screening of electrode materials, ranging from bioinspired moieties to synthetic metal-containing molecules to polycrystalline or single-crystal surfaces.

Among the noble metals, Pt has long been recognized for its high activity toward the reduction of nitrogen-containing molecules[7] and has been studied in detail, more recently also in the form of well-defined monocrystalline electrodes.[10,19,20] Within this field of study, the Leiden group has recently demonstrated a unique reactivity and selectivity at Pt(100) surfaces for nitrite reduction to N_2.[13] Not only does this achievement satisfy one of the requirements of electrochemical wastewater treatment (conversion of pollutant species into harmless dinitrogen), it also highlights the special ability of the Pt(100) surface in reactions involving bond breaking and bond making,[23] the selective oxidation of NH_3 to N_2[23−28] being one such example relevant for this study. In this reaction, highly stabilized ammonia fragments ($NH_{2,ads}$) recombine to give the intermediate N_2H_4, which is rapidly oxidized to N_2. This information was fundamental in proposing a tentative mechanism for selective nitrite reduction to N_2: the recombination of stable $NH_{2,ads}$ and NO_2^- at the surface was speculated,[13] although the detailed mechanistic events remained elusive.

Valuable clues to unraveling the steps leading to N_2 can be obtained by a comparison of nitrite reduction with two similar processes belonging to completely different research fields: the

Received: April 8, 2011
Published: May 31, 2011

so-called "anammox" (anoxic ammonia oxidation) bacterial sewage treatment[7,29,30] and the selective catalytic reduction (SCR)[31] of NO by NH_3 to N_2 under ultra-high-vacuum (UHV) conditions at a Pt(100) surface.[32−35] In the former, anoxic ammonium-oxidizing bacteria, naturally occurring in seawater, exploit an alternative path in the nitrogen cycle[30,36] by using NO_2^- obtained from enzymatic reduction of NO_3^- as an oxidizer in a further reaction that converts NH_4^+ to N_2. Isotope labeling experiments[29] in which nitrate was supplied as $^{15}NO_3^-$ demonstrated that recombination to $^{14}NH_4^+$ occurs, giving rise to mixed-isotope $^{14}N^{15}N$. These bacteria feature unique cellular components that are able to handle and withstand toxic, unstable N_2H_4; incidentally, we have noticed[7] that these bacteria and Pt(100) electrodes (see above) seem to have a similar pathway for ammonia oxidation.

SCR conversion of NO to N_2 at Pt(100) at high temperature has attracted much interest in the literature (recently reviewed by Hu et al.[31]) as concerns both the experimental behavior of this system under UHV conditions[31−34] and its theoretical simulation,[35,37,38] the latter mainly concerned with a rationalization of the oscillatory behavior observed during prolonged reaction. Adsorbed NO plays a very important role: there is compelling evidence that the hexagonal reconstruction of Pt(100) can be lifted upon NO adsorption, creating the (1 × 1) orientation, which is the only one active toward NO reduction to N_2 because it offers a favorable surface for the stabilization of NH_x fragments.[32,35,37] Although $\theta_{NO} > \theta_{NH_x}$ in all cases, due to the higher heat of adsorption of NO_{ads} on Pt(100), evidence of mutual stabilization of NO_{ads} and $NH_{x,ads}$ was found,[32,33] with the ensuing formation of $NO_{ads}-NH_{x,ads}$ ($x = 1-3$) complexes at the periphery of the NO islands, where the N_2 evolution preferentially occurs.[33] Isotope labeling experiments[32] using ^{15}NO and $^{14}NH_3$ have indeed evidenced the formation of $^{14}N^{15}N$, along with single-isotope $^{14}N^{14}N$ and $^{15}N^{15}N$. The determination of the elementary steps leading to N_2 need to take into account all temperature-dependent dissociation processes (NO decomposition, mainly),[31,34] and the accepted scheme can be summarized as

$$NO_{ads} \rightarrow N_{ads} + O_{ads} \quad (1)$$

$$\tilde{N}H_{3,ads} \rightarrow \tilde{N}_{ads} + 3H_{ads} \quad (2)$$

$$N_{ads} + \tilde{N}_{ads} \rightarrow \tilde{N}N \quad (3)$$

$$2H_{ads} + O_{ads} \rightarrow H_2O \quad (4)$$

where we have "labeled" the ammonia nitrogen $\tilde{N}$ in reaction 3 to indicate explicitly that N_2 may arise in principle from a recombination of two N atoms originating from any of the two reacting species. However, Hallock et al. have remarked[34] that, in view of the clear isotopic excess of $^{14}N^{15}N$ measured in the experiments at $T < 500$ K, and given that NO decomposition becomes much slower, the decomposition of the more labile NH_x fragments must be predominant below this temperature, supplying "reducing agents" (N_{ads}) to NO_{ads} in the following process:

$$\tilde{N}_{ads} + NO_{ads} \rightarrow N\tilde{N} + O_{ads} \quad (5)$$

which then represents the actual overall reaction leading to N_2 evolution.

This paper will elucidate the mechanistic origin of the unique reactivity of (100) sites toward nitrite reduction to N_2. By combining spectroelectrochemical studies and mass spectrometry experiments with isotope labeling, we will show that a low-temperature variant of the SCR mechanism is responsible for the high selectivity to N_2. In particular, $NH_{x,ads}$ and NO_{ads} will be identified as the key surface species that take part in a Langmuir−Hinshelwood recombination, which is the defining step of the overall mechanism leading to N_2. Additionally, the role of surface defects in decreasing the catalytic activity and selectivity to N_2 of the electrode will be discussed: quasi-perfect (100) domains are required to maximize nitrite conversion to N_2, providing useful hints for designing practical catalysts for this reaction. From a broader perspective, we demonstrate the intimate similarities of the "anammox-type" N_2 evolution in such diverse fields as electrocatalysis, fundamental surface science, and applied bacterial bioengineering. We will also briefly discuss the advantages of this type of N_2 formation over other known mechanisms, especially with regard to reaching the desired high selectivity.

Table 1. List of Single-Crystal Surfaces Used in This Study[a]

zone	Miller indices	terrace-step notation
[011]	(39,1,1)	20(100) × (111)
	(29,1,1)	15(100) × (111)
	(23,1,1)	12(100) × (111)
	(15,1,1)	8(100) × (111)
	(11,1,1)	6(100) × (111)
	(7,1,1)	4(100) × (111)
[001]	(20,1,0)	20(100) × (110)
	(15,1,0)	15(100) × (110)
	(10,1,0)	10(100) × (110)
	(7,1,0)	7(100) × (110)
	(5,1,0)	5(100) × (110)
	(4,1,0)	4(100) × (110)

[a] The notation in the rightmost column is n(terrace) × step, where n is the number of terrace atoms.

EXPERIMENTAL SECTION

Electrochemical Experiments. Platinum single-crystal electrodes were oriented, cut, and polished from small (2−3 mm diameter) single-crystal beads as reported previously.[39] The different electrodes used, including Miller indices, terrace-step notation, and crystallographic zone, are given in Table 1.

Before every experiment, the electrode was flame annealed and cooled in a reducing atmosphere containing H_2 + Ar[40] and protected with water in equilibrium with this gas mixture to prevent contamination before immersion in the electrochemical cell.[41] The counter electrode was a platinum spiral wire. Potentials were measured against a reversible hydrogen electrode (RHE) connected to the cell through a Luggin capillary. The electrolyte solutions were deoxygenated prior to the measurements with Ar (6.0); during the measurements, the penetration of oxygen into the cells was minimized with a continuous blanketing Ar flow. The voltammetric experiments were carried out in two classical three-electrode electrochemical cells, one of them containing the blank solution (namely, 0.1 M $HClO_4$) and a second one containing the test solution (0.1 M NaOH + 2 mM $NaNO_2$). The blank solution was used to characterize the electrode surface and determine the surface order. The electrode was rinsed and transferred to the test solution containing nitrite anions. So-called transfer experiments[14,42−44] were carried out according to the following procedure: a saturated NO adlayer at a Pt(100) electrode was produced following the method described by Rodes et al.,[44] in which the electrode must be immersed, at open circuit potential, into a 0.1 M $HClO_4$ solution containing 0.01 M $NaNO_2$ for 30 s. Less dense adlayers can be obtained by reducing the immersion

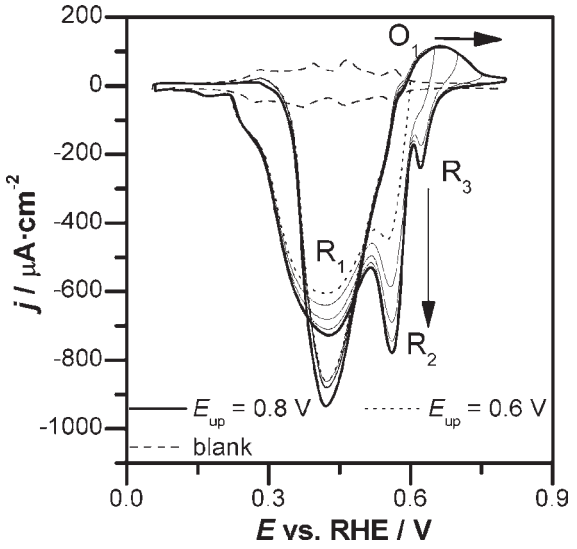

Figure 1. Cyclic voltammetry profiles for nitrite reduction at the Pt(100) surface in 0.1 M NaOH in the absence (dashed line) and in the presence of 2 mM $NaNO_2$. The starting potential E_{start} = 0.1 V, while the upper potential limit (E_{up}) is progressively increased to higher potentials. The dotted line refers to E_{up} = 0.6 V, the thick line refers to E_{up} = 0.8 V, and the thin lines refer to three selected intermediate potentials. The scan rate was in all cases 50 mV/s. For a description of the individual signals labeled in the figures, refer to the text.

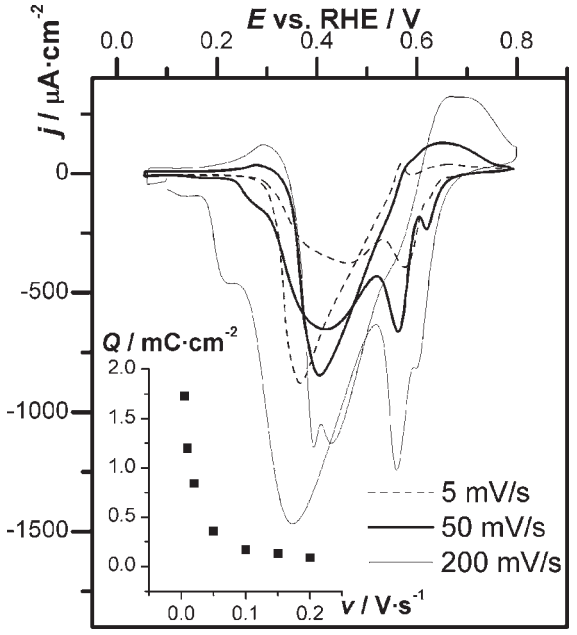

Figure 2. Cyclic voltammetry profiles for nitrite reduction at the Pt(100) surface in 0.1 M NaOH for various scan rates in the presence of 2 mM $NaNO_2$. The scan rate is v = 50 mV/s (thick line), v = 5 mV/s (dashed line), and v = 200 mV/s (thin line). The starting potential E_{start} = 0.1 V. The potential was first swept to 0.06 V and then reversed until 0.8 V. The inset displays the dependence of the charge of the peak at 0.55 V (R_2) on the scan rate.

time or the nitrite concentration. The electrode was then rinsed and transferred to the cell containing the working solution. NH_x adsorbates can be generated in a similar way as first described by De Vooys et al.,[45] by contacting the electrode with an ammonia-containing 0.1 M NaOH solution at constant potential (see below for more details). All the experiments were done at room temperature.

Electrolyte solutions were prepared from concentrated perchloric acid (Merck Suprapur), sodium hydroxide (Merck Suprapur), sodium nitrite (Sigma-Aldrich, 99.999%), and ultrapure water (Elga Purelab Ultra or Milli-Q Millipore, 18.2 MΩ cm). Labeled sodium nitrite was supplied by Cambridge Isotope Laboratory (15 N, 98+%). The measurements were performed with an EG&G 175 signal generator, an eDAQ EA161 potentiostat, and an eDAQ e-corder ED401 recording system.

Spectroelectrochemical Experiments. Fourier-transform infrared spectroscopy (FTIRS) experiments were performed with a Nicolet Magna 850 spectrometer, equipped with an MCT detector. The spectroelectrochemical cell was provided with a prismatic CaF_2 window beveled at 60°. Spectra shown are composed of 200 or 1000 interferograms (indicated in the figure) collected with a resolution of 8 cm^{-1} and p-polarized light. They are presented as absorbance, according to $A = -\log(R/R_0)$, where R and R_0 are the reflectances corresponding to the single beam spectra obtained at the sample and reference potentials, respectively.

All the spectroelectrochemical experiments were conducted at room temperature, with a reversible hydrogen electrode (RHE) and a platinum wire used as the reference and counter electrodes, respectively. The electrochemical cell and the electrolyte solutions were prepared as described in the previous section.

Online Electrochemical Mass Spectrometry (OLEMS). A detailed description of the setup can be found in previous publications.[14,46] In brief, the flame-annealed single-crystal electrode, protected by a droplet of Ar−H_2-saturated water, was exposed to the working electrolyte in a hanging-meniscus configuration under potential control, and a PTFE tip, connected to the mass spectrometer, was positioned at approximately 10 μm from the single-crystal electrode. The solution was not stirred during the experiments, and a flow of blanketing Ar was maintained to protect the solution from oxygen. All OLEMS experiments were carried out at a scan rate of 1 mV/s. The OLEMS setup does not allow a quantitative analysis of the signals. However, if the experiments are repeated with the same PTFE tip and at a comparable pressure (measured with a full-range pressure gauge), the relative magnitudes of ion currents measured prove to be highly reproducible. An internal, semiquantitative calibration can also be carried out, and further details will be reported below when the results are presented. The potential was controlled with a computer-controlled IviumStat potentiostat (Ivium Technologies).

RESULTS

Electrochemical Experiments. Figure 1 depicts the blank cyclic voltammetry of a well-ordered Pt(100) surface in NaOH (0.1 M) along with the voltammetric response in the presence of nitrite anions for successively increased values of the positive vertex potential (E_{up}).

Several features can be identified in the broadest voltammetric profile recorded from 0.06 to 0.8 V at 50 mV/s; for these values of E_{start} and E_{up} negligible faradic currents were measured at the two extremes of the potential window. In the first positive-going sweep, a major reduction peak at 0.4 V can be observed (R_1), followed by a broad oxidation peak at 0.55−0.75 V (O_1). Upon reversal of the scan direction at E = 0.8 V, several reduction signals can be observed in the negative-going scan. A minor peak at 0.63 V (R_3) is followed by a more intense peak at 0.55 V (R_2); the largest signal is still the broad peak centered at 0.4 V (R_1). On the basis of previous studies,[10,13] the following assignment of the peaks can be suggested: R_1 arises from direct nitrite reduction to ammonia,[10] whereas R_2 is ascribed to selective nitrite reduction

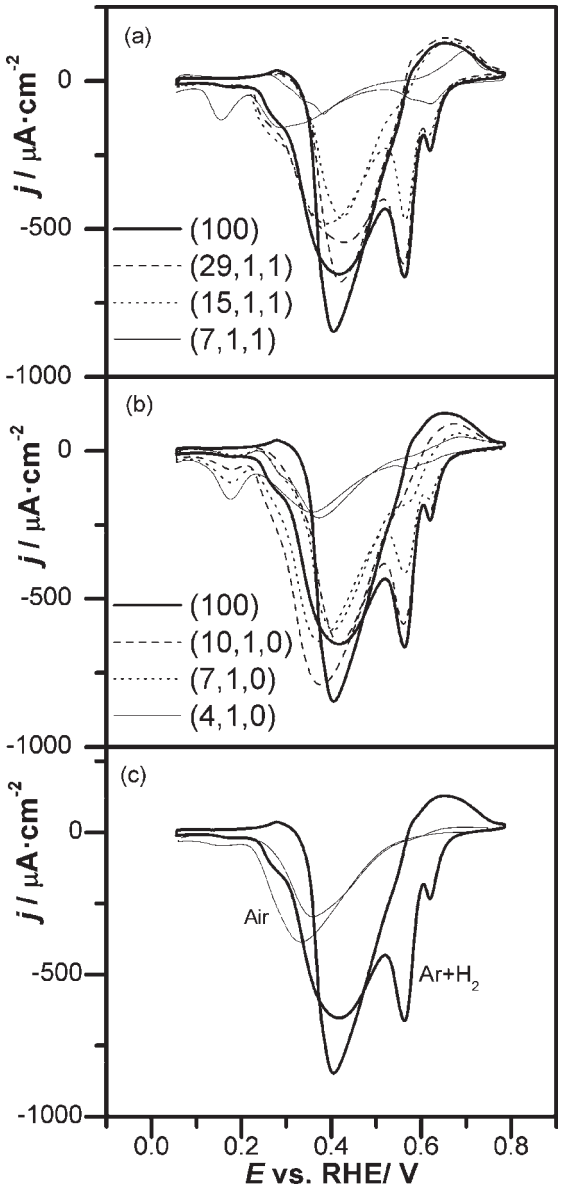

Figure 3. (a) Nitrite reduction profiles on selected Pt[(100) × (111)] surfaces: thick line, (100); dashed line, (29,1,1); dotted line, (15,1,1); thin line, (7,1,1). (b) Nitrite reduction profiles for selected Pt[(100) × (110)] surfaces: thick line, (100); dashed line, (10,1,0); dotted line, (7,1,0); thin line, (4,1,0). (c) Comparison between the voltammetric response of a Pt(100) electrode cooled in an argon + hydrogen atmosphere (thick line) and in ambient air (thin line). For the blank voltammogram of a well-ordered Pt(100) electrode, refer to Figure 1. For all three panels, $\nu = 50$ mV/s and the $NaNO_2$ concentration is 2 mM in 0.1 M NaOH.

to dinitrogen.[13] O_1 falls in the region where Ye et al.[10] observed reoxidation of ammonia, generated at R_1, to dinitrogen. The modification of the upper potential limit allows us to investigate the relationship between the various voltammetric features, and as depicted in Figure 1, there is a correlation between the growth of O_1 and the increase of R_2. The growth of the two signals is maximal when E_{up} is increased between 0.6 and 0.75 V, and at higher potentials they both level off to an almost constant value. Therefore, within the time scale of this specific electrochemical experiment, the oxidation of a particular intermediate, or surface

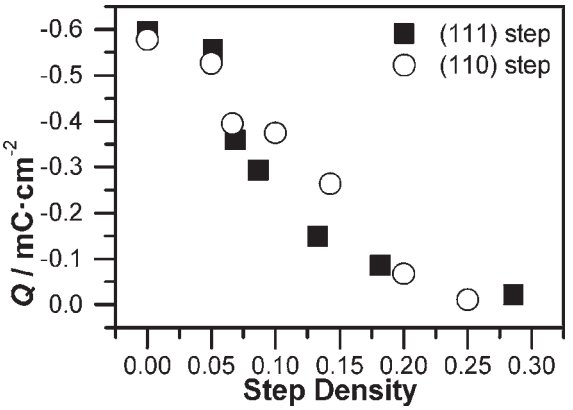

Figure 4. Peak charge of R_2. The peak integration was performed with voltammetric data recorded at $\nu = 50$ mV/s (starting potential $E = 0.1$ V, 2 mM $NaNO_2$). The step density has been calculated as $1/(n - 0.5)$ for (100) × (111) surfaces and $1/n$ for (100) × (110) surfaces. Values of n can be found in Table 1 for the various surfaces.

species involved in O_1, can enhance the ensuing reduction process R_2. Additional information on the nature of the various peaks can be discerned from a comparison of the voltammetric profiles at different scan rates, as shown in Figure 2.

All peaks are generally characterized by a decreased peak current with decreasing scan rate, although this decrease is less noticeable when the scan rate is reduced from 50 to 5 mV/s. It should be noted that R_3 disappears at the lowest scan rate, which is in agreement with the previous report[13] where it was not observed at 1 mV/s. Therefore, it can be assumed that R_3 is a shoulder of the main reduction process of peak R_2. We shall now discuss the behavior of R_2 and O_1 in more detail. The R_2 peak potential does not shift noticeably within the range of ν values analyzed (only a 15 mV shift across a two-decade range); on the other hand, the peak charge follows the trend shown in the inset of Figure 2: the amount of charge measured remarkably increases with a decrease of the scan rate (that is, with an increased experimental time scale). The trend is best fitted by an exponential decay. Our results agree with previous observations by the Kita group,[10] who noticed that the charge of R_1 also increases with a decrease in scan rate. Therefore, the overall process giving rise to R_2 must include a slow surface-confined step. On the other hand, we interpret the increase of the peak current of O_1 with the scan rate as a consequence of a process involving a species that can diffuse away from the electrode unless the time scale of the potential sweep is short enough. As we mentioned above, we identify this species with NH_3 produced in the R_1 region.

To probe the importance of long-range (100) facets for the selective reduction of NO_2^-, we have also studied the effect of the introduction of steps of known orientation into the (100) structure. The voltammetric profiles of nitrite reduction of some of these stepped surfaces are shown in parts a and b of Figure 3 for the (111) and (110) step orientation, respectively. The peak pattern of the (100) electrode is largely conserved, but the magnitude of all signals decreases with an increasing step density, regardless of the orientation of the step. This effect affects all peaks, although to different extents. The large reduction peak at ca. 0.4 V, associated with the formation of ammonia, also does not decrease remarkably when surfaces with long terraces are used. The oxidation signal above 0.6 V does not shrink appreciably when (111) steps are introduced unless a high step density

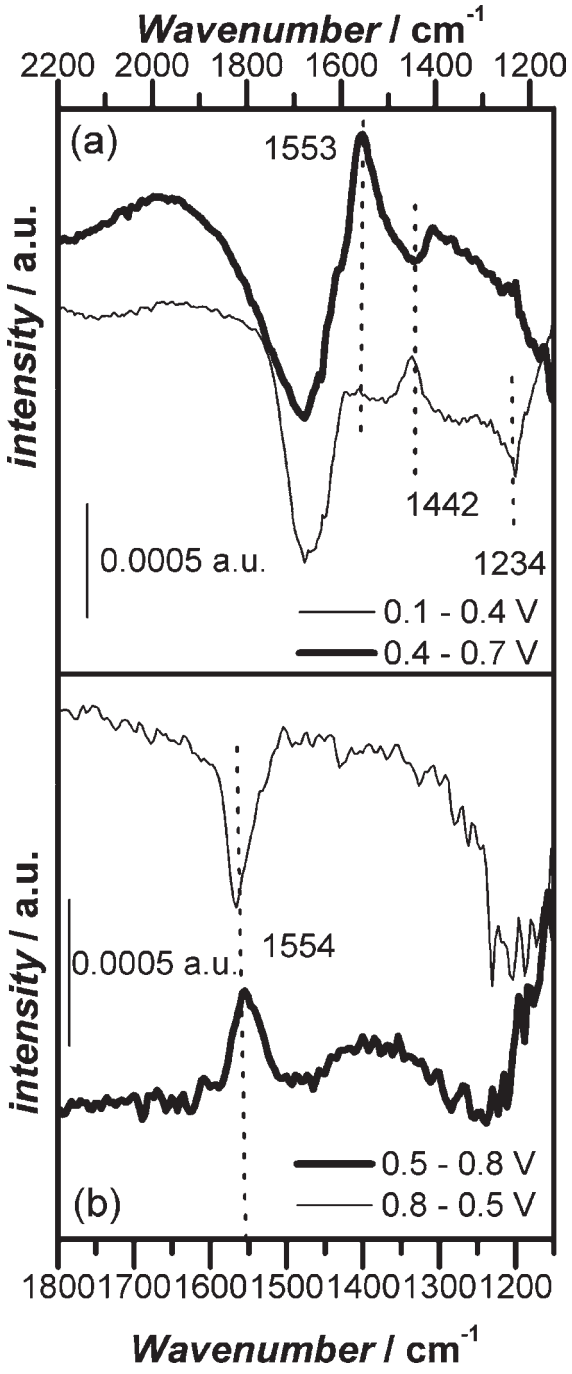

Figure 5. (a) FTIRS spectra for nitrite reduction at Pt(100) in a 0.1 M NaOH solution containing 2 mM $NaNO_2$. A total of 1000 interferograms were collected with a resolution of 8 cm^{-1}. Thin line: reference potential 0.1 V and sample potential 0.4 V. Thick line: reference potential 0.4 V and sample potential 0.7 V. (b) FTIRS spectra for nitrite reduction in 0.1 M $NaOH/D_2O$ containing 2 mM $NaNO_2$. A total of 200 interferograms were collected with a resolution of 8 cm^{-1}. Thin line: reference potential 0.5 V and sample potential 0.8 V. Thick line: reference potential 0.8 V and sample potential 0.5 V.

is reached. The trend of the peak charge of R_2 with respect to the step density is shown in Figure 4. The introduction of steps dramatically reduces the corresponding charge, with a noticeable decrease even for low step densities. We conclude that only surfaces with long-range-ordered two-dimensional (100) domains are able to reach the maximum catalytic activity toward N_2 evolution from nitrite, and the interruption of such long-range order with defects, even if (100) terraces are very long along the steps, reduces the activity of the Pt surface.

The importance of high-quality (100) facets was further corroborated by an additional experiment involving a nonoptimal procedure of electrode pretreatment, which will prevent the surface from reaching an ideal (100) orientation by inducing various types of defects.[40,47−49] Using Pt(100), we performed flame-annealing as described in the Experimental Section, followed by cooling in ambient air rather than in a controlled oxygen-free atmosphere. The activity toward nitrite reduction of the electrode was then tested and compared to that of a well-ordered (100) electrode. Figure 3c shows the voltammetric profile of such "air-cooled" Pt(100). The peak related to N_2 evolution has completely disappeared, along with the oxidation signal recorded above 0.6 V. The reduction peak associated with ammonia formation is still present, although it features a much lower peak current and a less positive peak potential with respect to the crystal cooled in an argon + hydrogen atmosphere. We also note that the profile of the air-cooled crystal shows a close similarity to the voltammogram previously published by Ye et al.[10]

Spectroelectrochemical Experiments: FTIRS of (100) and Selected Stepped Surfaces. In situ IR spectroelectrochemistry has been employed for the identification of possible reaction intermediates and can be applied to single-crystal surfaces (in the external reflection configuration). IR-active vibrations assigned to (adsorbed) NO,[43,44,50] NO_2^-,[44] NO_3^-,[17,21] and NH_x fragments[42] have previously been observed with a comparable configuration. In the following spectra, the positive bands correspond to the products formed during the reaction, while negative bands arise due to the consumption of species present at the reference potential. The electrodes were always brought into contact with the nitrite solution at controlled potential (0.1 or 0.8 V) where negligible faradic current is measured. After collection of the reference spectrum, the potential was progressively stepped to the sample potentials: these values are reported in the corresponding figures and captions (see below).

As an additional comment, the IR experiments were performed in the thin layer configuration, and it was observed that the gas formation—in our case N_2 evolution—disturbed the acquisition of the optical signal through the thin layer. Therefore, no IR spectra could be acquired in the region corresponding to gas formation, more precisely 0.5 V < E < 0.65 V. However, selected experiments were performed with a reference potential just outside this window to compare the electrode surface state at the two extremes of the N_2-forming region. Additionally, the reference potential was selected as close as possible to the sample potential to minimize the influence of the water bands on the spectra (potential-driven modification of the water configuration in the thin layer). This is especially important when a continuous reaction is studied, for which reactant depletion may arise in the thin-layer configuration. On the other hand, such a configuration is ideally applicable to simpler cases such as the removal of an adsorbed species from the electrode surface.

Figure 5a displays two results of FTIR spectra for Pt(100) in the presence of NO_2^-. Four bands are clearly observed in the spectra: the signal at 1640 cm^{-1} corresponds to water bending[51] and arises from the water depletion from the thin layer; the other bands can be attributed to the N−O_{ads} stretching mode (1553 cm^{-1}),[44] N−H bending mode (1442 cm^{-1}),[42] and asymmetric NO_2^- bending mode (1234 cm^{-1}).[44,51,52] If the

Scheme 1. Stability Potential Ranges of $NH_{x,ads}$ and NO_{ads}[a]

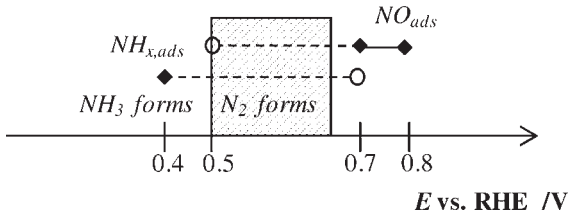

[a] The full tilted square indicates a potential corresponding to FTIRS evidence of the *formation* of a surface species, while the empty circle indicates a potential corresponding to FTIRS evidence of the *removal* of the species. The region of gas evolution, where no FTIRS data can be collected, is highlighted as a shadowed rectangle. The potential axis is not to scale.

potential is stepped from a reference starting potential of 0.1 to 0.4 V, we observe that the band assigned to NH_x species is positive, which means that NH_x species are produced at 0.4 V with a simultaneous depletion of solution-phase nitrite, a process highlighted by the negative band at 1234 cm^{-1}. Subsequently, when the potential is stepped from 0.4 to 0.7 V across the N_2 formation region, the band at 1442 cm^{-1} becomes negative, indicating that NH_x species are removed from the thin layer at 0.7 V with respect to 0.4 V. This process is accompanied by the appearance of a positive band related to adsorbed NO. Therefore, this experiment shows that various processes take place at the Pt(100) electrode along the sequence 0.1 V → 0.4 V → 0.7 V: first conversion of nitrite to "N−H" species, presumably also involving NH_3, then removal of these N−H species and the appearance of surface NO.

Although the band related to adsorbed NO is unambiguous, the interference of the neighboring water band was removed by repeating the experiment in the presence of D_2O. In this way, the water bending signal is displaced to lower wavenumbers.[53] We were then in the condition to perform an accurate experiment aimed at determining the potential at which this band disappears, signaling the removal of the NO adsorbed at the surface. The experiment in D_2O adds little information about other bands, for example, the nitrite bending, which are now masked by the D_2O signal. Figure 5b displays the results of a potential-step FTIRS experiment in D_2O. When the reference potential is chosen as close as possible to the N_2 region (0.5 V) and then stepped to the working potential (0.8 V), a positive band corresponding to the appearance of NO_{ads} is observed, consistent with the results displayed in Figure 5a. If a new reference spectrum is acquired and the potential is then returned to 0.5 V, the NO band changes sign, showing removal of this species. When taken together, the FTIRS experiments in regular and heavy water allow us to highlight the *identity* of the key surface species involved in nitrite reduction ($NH_{x,ads}$ and NO_{ads}) and their *stability potential ranges*, which are summarized in Scheme 1.

The stability potential ranges are necessarily discontinuous because of the stepped potential programs employed in FTIRS experiments. Scheme 1 depicts this fact by showing the *possible* stability ranges as dotted lines. Despite this fact, and the presence of a wide potential window where FTIRS data cannot be collected, we can unambiguously affirm that NH_x fragments are the dominant surface species for $E < 0.4$ V while NO predominates when $E > 0.7$ V. Further FTIRS experiments were aimed at determining the influence of the surface structure on the identity

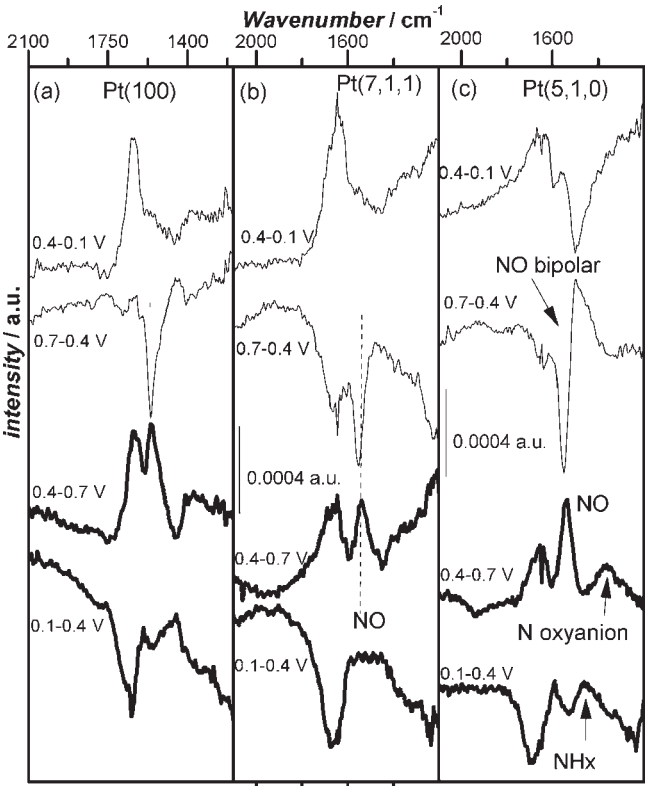

Figure 6. Spectra for nitrite reduction on Pt(100), Pt(7,1,1), and Pt(5,1,0) in 0.1 M NaOH and 2 mM $NaNO_2$ in H_2O. A total of 200 interferograms were collected with a resolution of 8 cm^{-1}. The potential program involved a staircase with the following steps: 0.1 V → 0.4 V → 0.7 V → 0.4 V → 0.1 V. The thick lines represent the positive-going direction (from 0.1 to 0.7 V) and thin lines the negative-going direction (from 0.7 to 0.1 V).

and the stability of the surface intermediates: Pt(7,1,1) and Pt(5,1,0) were selected as model stepped surfaces. Their FTIR spectra are shown in Figure 6.

The experiment shown in Figure 6 involves a complete sweep between 0.1 and 0.7 V, performed by means of the following stepwise potential program: 0.1 V → 0.4 V → 0.7 V → 0.4 V → 0.1 V. For every step, a new reference potential was acquired at the starting E value. As an additional difference from the experiment reported in Figure 5a, the number of interferograms acquired is much smaller: this choice is advantageous because it allows a faster data acquisition, but it suffers from the drawback that vibrations related to NH_x and nitrite are somewhat less intense than in Figure 5, and the very intense vibration of NO_{ads} dominates the spectra of Figure 6. As the spectra of Pt(100) are in agreement with those of Figure 5, we concentrate on the spectra of Pt(7,1,1) and Pt(5,1,0). The spectroelectrochemical analysis of the Pt(7,1,1) surface, displayed in Figure 6b, reveals that no NH_x bands at 1449 cm^{-1} are observed upon stepping the potential from 0.1 to 0.4 V, suggesting a more limited nitrite consumption, in agreement with the voltammetric data of Figure 2, where Pt(7,1,1) features a much lower reduction current at R_1 than Pt(100). The second step to 0.7 V shows that the stepped surface generates less NO than the basal plane, as demonstrated by the weaker NO band observed. However, the conservation of the band position indicates that the adsorption coordination is the same on both Pt(7,1,1) and Pt(100), i.e., a multifold coordination on

(100) domains. NO is subsequently removed when the potential is stepped again to lower values, as expected.

In the case of the Pt(5,1,0) surface (having 110 steps), a small band related to NH_x species can still be observed after the first step to 0.4 V: a partial contribution of the fairly reactive (110) sites[10,13] for the reduction of nitrite to ammonia cannot be excluded. At 0.7 V, the NO band can be observed, along with another band at 1357 cm^{-1}. This band can be assigned to the asymmetric bending of adsorbed nitrite in a "nitro" configuration (M−N coordination)[17,54] or to solution-phase nitrate.[52] We favor the former assignment, with (110) sites most likely being involved in the adsorption of nitrite. When the potential is stepped back to 0.4 V, no NO consumption is observed; on the contrary, NO is still present and adsorbed at the surface as indicated by the bipolar band. The NO is only stripped from the surface at potentials lower than 0.4 V and can only be removed in the last step to 0.1 V. This is most likely related to the high affinity of NO toward step sites of (110) geometry, as reported in previous works.[7]

The spectroelectrochemical experiments on short-terrace stepped surfaces shed additional light on the origin of the decrease in reactivity as a result of the introduction of steps on (100) terraces: (111) steps cause a diminished conversion of nitrite into both $NH_{x,ads}$ and NO_{ads}, thus acting as inert surface domains. On the other hand, (110) steps do not depress the formation of NH_x while displaying a high affinity toward both NO_2^- and NO, the latter residing at the surface across the potential region of N_2 formation; therefore, this may suggest that (110) domains are the favorite adsorption sites for NO, where it is firmly bound and consequently excluded from further reaction at the (100) terrace. In other words, (110) steps could be described as self-poisoned as long as NO is bound.

OLEMS Experiments with (100) Electrodes and Selected Stepped Surfaces. The activity and selectivity series obtained by cyclic voltammetry was further corroborated by a study of the influence of the step density on the MS ion current related to N_2 (m/z = 28). During the measurements, m/z = 28 was the only mass recorded to optimize the signal intensity: we should however remark that a preliminary OLEMS experiment including also m/z = 30 (NO, N_2O) and m/z = 44 (N_2O) confirmed that for a (7,1,1) surface no gaseous product other than N_2 is formed during nitrite reduction, which can confidently be assumed to be true for surfaces with larger terraces as well (our previous studies[13] on Pt(100) also excluded other gaseous side products). Although the OLEMS setup has some intrinsic limitations to a quantitative analysis, a semiquantitative comparison of different experiments can still be carried out, and a correction was introduced by measuring the steady-state ion current related to hydrogen evolution, m/z = 2 at E = −0.1 V for all electrodes at the end of the experiment, without changing the geometry (i.e., tip−electrode distance) of the system.

Figure 7 shows the m/z = 28 normalized peak heights ($I^* = I/I_{normalization}$) and areas ($A^* = A/I_{normalization}$) for the positive-going (from 0.1 to 0.8 V) and the negative-going half-cycles as a function of the step density of selected surfaces from (100) down to large, medium, and small terrace widths for both (111) and (110) steps (see Table 1 for additional information).

The figure shows that, irrespective of the parameter employed (peak height or area) or the scan direction analyzed, the amount of N_2 formed during the potentiodynamic cycle is strongly dependent on the step density: for surfaces with wide terraces such as (39,1,1) and (20,1,0), the magnitude of N_2 evolution already decreases by more than 50% with respect to the (100)

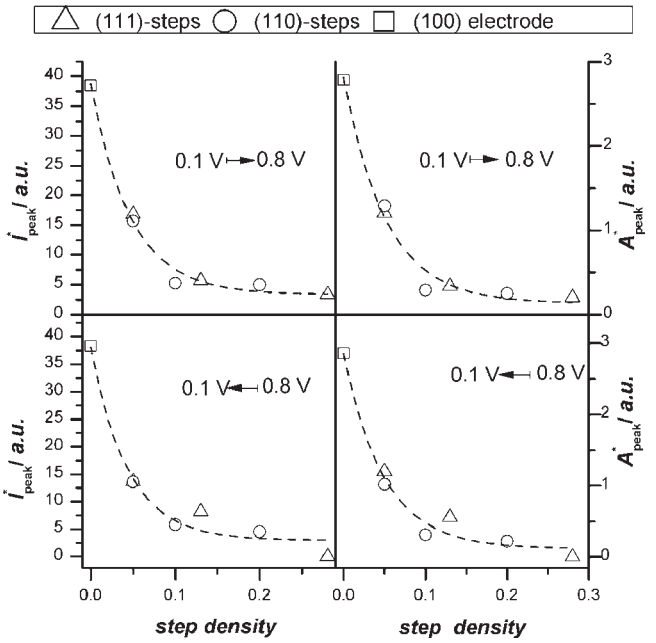

Figure 7. OLEMS data for N_2 evolution on the stepped surfaces investigated in this paper. Squares refer to the (100) electrode, triangles to surfaces featuring (111) steps, and circles to those with (110) steps. Two peak parameters are reported. The left column contains the normalized peak height (I^*) for both the positive- and the negative-going scans. The right column contains the normalized peak area (A^*). For both parameters a nonlinear fitting was performed using an exponential decay function, displayed in the figure as dotted lines. All OLEMS data were collected during potential scans with E_{start} = 0.06 V and v = 1 mV/s.

surface. An additional increase in the step density causes a further decrease of the intensity of the N_2 MS peak until the lowest values are reached for (7,1,1) and (5,1,0) surfaces. In fact, the (7,1,1) electrode evolves an amount of N_2 very close to the detection limit of the OLEMS setup in the positive-going scan and below this limit in the negative-going scan (see Figure 7). The trend reported in Figure 7, which can qualitatively be fitted by an exponential decay, can be positively compared to the plot in Figure 3, although the electrochemical analysis and the OLEMS experiments were carried out in different conditions. Consequently, it is by no means surprising that the trends of Figures 3 and 7 are not identical, the latter showing a much more abrupt decrease of the MS peak parameters for N_2 evolution even with very small step densities. However, both techniques agree on the limiting terrace width for a detectable N_2 evolution (four atoms), and the mass spectroscopy data corroborate the observation that steps—regardless of their symmetry—exert a deleterious effect on the reaction pathways leading to N_2.

An additional experiment was carried out to analyze the catalytic performance of one-dimensional (100) sites, aimed at determining the smallest (100) domain active toward N_2 evolution. A suitable [n(111) × (100)] single-crystal electrode was chosen, in our case (533), having n = 10. Although a reduction current was indeed recorded in the potential region typical of nitrite reduction at (111) sites, no N_2 was simultaneously detected in the OLEMS apparatus. Therefore, we can exclude that one-dimensional (100) steps are active toward N_2 evolution, which instead requires wide two-dimensional (100) domains.

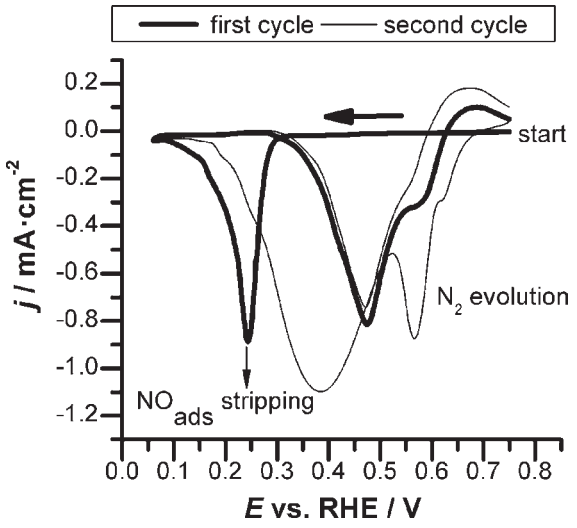

Figure 8. Voltammetric profile of a NO-saturated Pt(100) electrode in a 0.1 M NaOH solution containing 2 mM $NaNO_2$: first scan, thick line; second scan, thin line. E_{start} = 0.75 V, and ν = 50 mV/s.

Transfer experiments with NO and NH_x. Mass Spectrometry and Electrochemical Results. Since NO was observed with FTIRS during nitrite reduction at Pt(100), we performed an electrochemical "transfer" experiment to probe the influence of the presence of a saturated NO adlayer (prepared as specified in the Experimental Section) on N_2 evolution. In this experiment the presence or the absence of the R_2 peak was considered as the only evidence of generation of this gas at this stage. A saturated coverage of NO of ca. 0.5 monolayer[55,56] has been estimated for Pt(100) under electrochemical conditions. The NO-covered electrode was contacted with a nitrite-containing 0.1 M NaOH solution at E = 0.8 V, and a potential sweep in the negative direction was started. The two subsequent voltammetric scans are shown in Figure 8.

The reduction profiles of the electrode are clearly different in the first and second cycles. During the first sweep, with the electrode fully covered with NO, no reduction current is detected until 0.25 V, which can be ascribed to NO_{ads} reductive stripping.[44] Upon reversal of the potential scan, the broad reduction peak R_1 reappears, and in the following second cycle, R_2 can be observed again. The removal of NO from the surface is not complete with the fast scan rate employed. Hence, a residual, very low coverage of NO may still be present, but it was not found to be deleterious for the reaction leading to N_2.

A more detailed analysis of the role of adsorbed NO was carried out using labeled $Na^{15}NO_2$. Our aim was to determine the fate of adsorbed ^{15}NO at Pt(100) during reduction of $Na^{14}NO_2$ in 0.1 M NaOH. Figure 8 shows the ion current traces for m/z = 28 ($^{14}N_2$) and m/z = 29 ($^{14}N^{15}N$), along with the voltammetric profile recorded during OLEMS experiments.

The ^{15}NO-covered electrode is not completely inhibited toward N_2 evolution, in contrast with the behavior observed during standard electrochemical measurement shown in Figure 8: this fact is ascribed to the known tendency of NO_{ads} to desorb from the Pt(100) surface in alkaline media during long experimental time scales.[44] However, here it is important to emphasize there is still a residual degree of electrode poisoning, evidenced by the smaller ion current for $^{14}N_2$ recorded in the first (negative-going) half-cycle with respect to the positive-going one. Notwithstanding

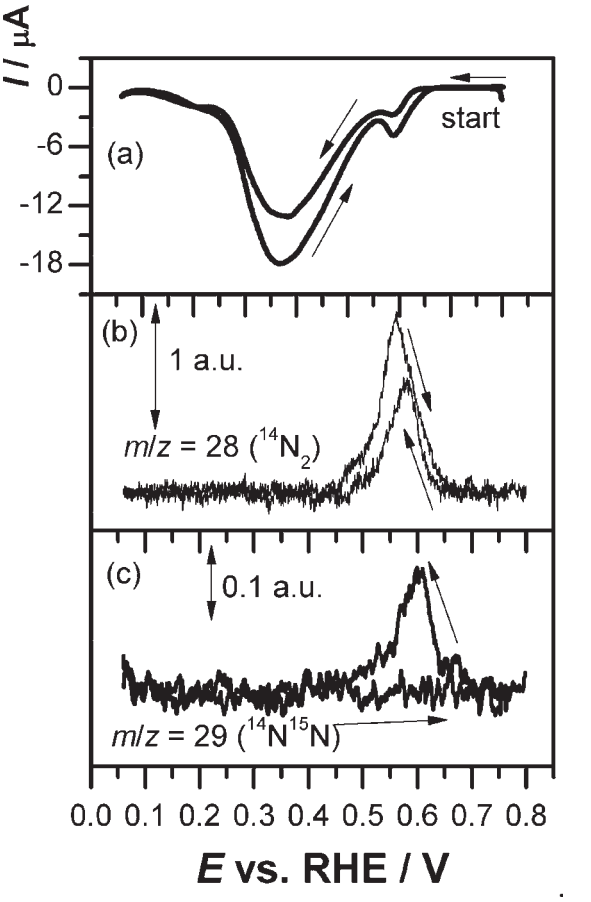

Figure 9. (a) Cyclic voltammetry during OLEMS measurements in a 0.1 M $Na^{14}NO_2$ solution following adsorption of ^{15}NO at a Pt(100) electrode. (b) Ion current profiles for m/z = 28. (c) Ion current profiles for m/z = 29. The arrows indicate the direction of the potential sweep. E_{start} = 0.8 V, and ν = 1 mV/s.

this residual poisoning, N_2 can be observed and a certain amount of $^{14}N^{15}N$ is also detected, which amounts to ca. 10% of $^{14}N_2$. This fact testifies that the surface ^{15}NO takes part in a reaction process involving a recombination with a ^{14}N species which must have originated from the solution-phase nitrite. All labeled NO is consumed in the first sweep, because no $^{14}N^{15}N$ is measured in the positive-going scan. The m/z = 30 ion current was found to be zero throughout the experiment, which shows that $^{15}N^{15}N$ potentially arising from a recombination of two ^{15}NO molecules cannot be detected (or is below the instrumental detection limit)

A second experiment was designed to probe the role of adsorbed NH_x, which we detected during FTIRS experiments. It is known[24] that such a fragment can be adsorbed onto a Pt(100) electrode from an alkaline solution of ammonia in the potential range of NH_3 oxidative adsorption (which proceeds via a dehydrogenation step to adsorbed NH_x fragments). The potential window of stability of NH_x fragments is roughly 0.35 V < E < 0.5 V. In addition, a previous publication has shown that transfer experiments involving NH_x species are feasible.[45] NH_x fragments were adsorbed from a $^{14}NH_3$ solution at a constant potential (E = 0.45 V) and transferred to a second electrochemical cell containing labeled $Na^{15}NO_2$. Figure 10 displays the ion current traces for m/z = 29 ($^{14}N^{15}N$) and m/z = 30 ($^{15}N_2$), along with the voltammetric profile recorded during the OLEMS experiment.

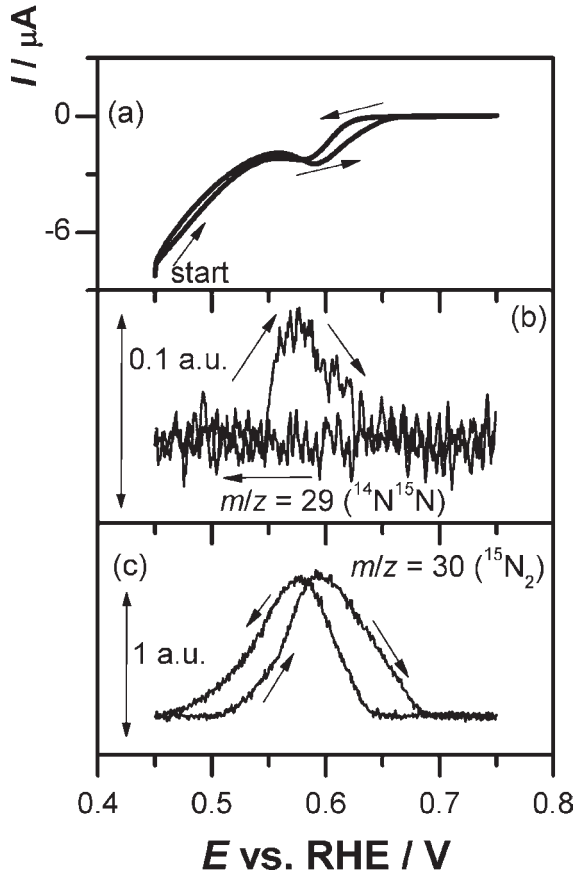

Figure 10. (a) Cyclic voltammetry during OLEMS measurements in a 0.1 M $Na^{15}NO_2$ solution following adsorption of $^{14}NH_x$ at a Pt(100) electrode. (b) Ion current profiles for $m/z = 29$. (c) Ion current profiles for $m/z = 30$. The arrows indicate the direction of the potential sweep. $E_{start} = 0.45$ V, and $\nu = 1$ mV/s.

During the voltammetric scan, started at $E = 0.45$ V, evolution of $^{15}N_2$ is observed in both cycles, with no clear poisoning effect. However, the formation of $^{14}N^{15}N$ is detected only in the first (positive-going) half-cycle, whereas no signal related to this molecule is recorded in the negative-going sweep. Therefore, the $^{14}NH_x$ fragments adsorbed on the surface recombine with another labeled moiety originated from the solution-phase labeled nitrite, thus giving rise to $^{14}N^{15}N$. It must be pointed out that no $^{14}N_2$ is detected: the recombination of $^{14}NH_x$ fragments does not take place or is below the sensitivity of the instrument.

DISCUSSION

The mechanistic analysis of nitrite reduction at Pt(100) is intimately correlated with the structure sensitivity of this reaction, and we shall therefore discuss the two topics alongside. The following discussion will be mainly devoted to the mechanism of N_2 formation.

Mechanism and Structure Sensitivity of Nitrite Reduction at Pt(100) Electrodes. FTIR evidence presented in this paper supports the presence of two key surface species at potentials vicinal to the potential window where N_2 evolution occurs: NO_{ads} and $NH_{x,ads}$. The direct involvement of both surface species in N_2 formation was further corroborated by the OLEMS experiment with labeled compounds. Scheme 1 (see above) showed the stability potential ranges of these species. A survey of literature

Scheme 2. Potential Ranges of Stability for $NH_{2,ads}$ and NO_{ads} Obtained from a Combination of Experimental Data from the Present Work and Literature Information[a]

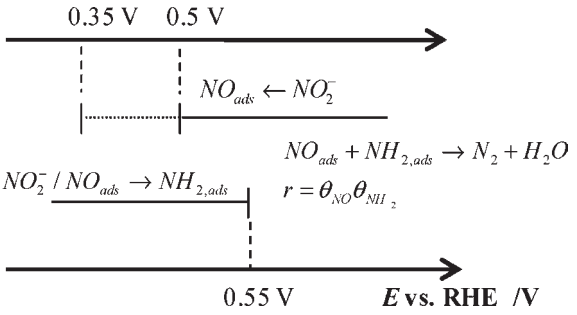

[a] The continuous line indicates the stability range for a certain molecule, along with the reaction that leads to this molecule starting from nitrite (see the text). The dotted line indicates, when needed, the theoretical stability range of a surface species in the absence of nitrite in the solution. The recombination reaction giving N_2 is highlighted, along with the simplest rate equation according to a Langmuir–Hinshelwood model. The potential axis is not to scale.

data concerning NO_{ads} and $NH_{x,ads}$ at Pt(100) electrodes in alkaline media allows us to obtain information about the potential region inaccessible to FTIRS investigation, thus enabling us to integrate and extend Scheme 1. The new scheme (Scheme 2) will be discussed in the next paragraphs.

Scheme 2 displays $NH_{x,ads}$ as $NH_{2,ads}$: in fact, Rosca et al. presented evidence for the presence of $NH_{2,ads}$ as the dominant intermediate during NH_3 oxidation at Pt(100) in alkaline media.[24] DFT calculations have shown that this ammonia fragment is characterized by a larger adsorption energy at Pt (100) surfaces than other NH_x species, providing extra stabilization to NH_2 on Pt(100) compared to other basal planes.[57,58] In addition, previous electrochemical experiments evidenced that this fragment is stable from 0.35 to ca. 0.55 V. At 0.55 V a large oxidation signal ascribed to bulk NH_3 oxidation predominates in the voltammogram,[24,27] and all $NH_{2,ads}$ is likely to be oxidatively removed. The first reduction peak of nitrite reduction (R_1), located within the stability range of $NH_{2,ads}$, may therefore generate such a fragment according to the following reaction:

$$4H_2O + NO_2^- + 5e^- \rightarrow NH_{2,ads} + 6OH^- \quad (6)$$

The second surface species, NO_{ads}, has been previously studied as an adsorbate at Pt(100) in clean 0.1 M NaOH by Rodes et al.,[44] who showed that the potential window of stability of NO_{ads} features a lower limit at $E = 0.35$ V. In addition, the adsorbate is not stable during long-term experiments, showing a tendency to desorb over time, which testifies that NO is a fairly labile adsorbate at Pt(100) in alkaline media. Combining this information with experimental evidence from Scheme 1, it seems reasonable to estimate that NO_{ads} may exist throughout the N_2 formation region up to 0.5 V: this is the E value where we obtained clear FTIRS evidence of the removal of this species. The conversion of solution-phase nitrite into NO will therefore be the dominant process for potentials higher than 0.65 V:

$$H_2O + e^- + NO_2^- \rightarrow NO_{ads} + 2OH^- \quad (7)$$

Scheme 2 shows that there is an intermediate region where the potential ranges of stability of the two products overlap and, consequently, interconversion of these species may occur. In

particular, as it is known that adsorbed NO forms NH_3 as the final product during reductive stripping,[7,44] it is logical to expect that the following reaction may occur in the overlap region where $NH_{2,ads}$ is stable:

$$NO_{ads} + 4e^- + 3H_2O \rightarrow NH_{2,ads} + 4OH^- \quad (8)$$

The presence of a central potential region, satisfactorily close to the observed R_2 peak potential, where the coexistence of NO_{ads} and $NH_{2,ads}$ can confidently be expected, suggests that a Langmuir−Hinshelwood recombination may be the fundamental step leading to N_2:

$$NO_{ads} + NH_{2,ads} \rightarrow N_2 + H_2O \quad (9)$$

Although this reaction may not be a truly elementary step (the nature of which cannot be concluded from experimental data presented in this paper), this is the most likely process responsible for N_2 evolution, also in light of the similar recombination that occurs between NO and NH_3 under UHV conditions. The choice of $x = 2$ for the NH_x fragment is mainly supported by experimental observations in previous papers (see above) concerning NH_2 stability on Pt(100) surfaces: in support of reaction 9 ab initio and thermochemical calculations[59−61] have also shown that other recombination reactions generating N_2, such as NH + NO, proceed via a much more unfavorable energetic pathway; NH_2 + NO, on the other hand, is characterized by the formation of a fairly stable NH_2−NO complex as the first step, whose existence during the UHV NH_3 + NO reaction was mentioned in the Introduction. For the latter reason, it may be possible that the role of NO_{ads} at Pt(100) is dual: reactant as well as stabilizer for $NH_{2,ads}$.

Scheme 2 also clearly shows that when the potential is changed in the positive- or negative-going direction, either $NH_{2,ads}$ or NO_{ads}, respectively, is already available at the surface from previous processes and, for reaction 9 to occur, the other reactant must be supplied in situ from an ancillary reaction of solution-phase nitrite, in agreement with isotope labeling experiments. This is best understood if the various processes occurring during the voltammetric scan, shown in Figure 1 and—for the slowest scan rate—Figure 9, are interpreted in light of Scheme 2. If the potential is swept from left to right, after R_1 the surface will be covered with $NH_{2,ads}$; two processes can in principle compete for the removal of the adsorbed species, reaction 9 or oxidative N_2 formation as observed during bulk NH_3 oxidation at Pt(100):

$$2NH_{2,ads} + 4OH^- \rightarrow N_2 + 4H_2O + 4e^- \quad (10)$$

Reaction 10 will dominate in the absence of coadsorbed NO and give rise to the voltammetric peak named O_1. Experimental evidence found in this work indicates that the scan rate plays a crucial role in steering the selectivity. At fast scan rates, reaction 10 dominates, along with oxidation of solution-phase NH_3 that is lingering in the proximity of the electrode and has not diffused into the bulk yet. Slower scan rates, on the other hand, allow reaction 7 to occur, providing an alternative pathway (i.e., reaction 9) for the removal of $NH_{2,ads}$. The correlation between voltammetric peaks O_1 and R_2 shown in Figure 1 can now be fully appreciated: as the upper potential limit is extended upward, the potential excursion will traverse an increasingly broader section of the potential window where reaction 7 predominates. In turn, this can cover the surface with a larger amount of NO_{ads} which, upon potential inversion, will be readily available to take part in N_2 evolution as soon as some $NH_{2,ads}$ has formed.

Finally, we comment on the structure sensitivity of nitrite reduction, concentrating on the most structure-sensitive process: R_2 (R_1, on the other hand, is still present when low-quality (100) domains are produced by air-cooling after flame-annealing, so lower quality (100) sites suffice for this reaction). The peculiarities of NO and NH_2 adsorption at (111), (110), and (100) sites can help with the interpretation of the structure sensitivity. $NH_{2,ads}$ has already been discussed above: the (100) plane features an outstanding stabilization of this fragment. Thus, steps of any symmetry would simply remove productive (100) surfaces and destabilize the $NH_{2,ads}$ adlayer. NO, on the other hand, is known to be fairly strongly adsorbed at Pt(110) sites, so we can imagine that reaction 7 is operative on this surface, too; however, NO is possibly a strongly adsorbed intermediate and thereby prevented from taking part in recombination (reaction 9). Indeed, the (5,1,0) surface gave rise to clear FTIRS evidence of the presence of NO in a broader potential region, as low as $E = 0.4$ V. On the other hand, (111) sites seem the least able to perform reaction 7, as indicated by the decreased NO FTIRS band (Figure 6). Consequently, the (100) surface possibly offers a "golden mean" situation, by performing reaction 7 at an adequate rate but without stabilizing NO excessively and without achieving a saturated NO adlayer which would poison the Pt(100) surface (Figure 8). A combination of these factors must contribute to determine the special behavior of Pt(100), which is the only Pt basal plane able to feature the coexistence of the two nitrogen moieties responsible for N_2 formation. As a more general comment, Pt(100) is an intrinsically unique surface, given its ability to promote reactions involving bond breaking or bond making: contrary to reactions needing low-coordination sites (i.e., steps) to promote the formation of a certain intermediate, the key to the high catalytic activity of Pt(100) is the extra stabilization given to the transition state with respect to the reactants' configuration.[23] Any surface defect acts as a hindrance and reduces the benign effect of a pristine Pt(100) surface. In our case, we have already mentioned that NO is likely to be only sufficiently stable as an adlayer at Pt(100) in alkaline media, while $NH_{2,ads}$ reacts to give N_2 in a potential region where it is prone to various transformations. All these factors contribute to the efficiency of this pathway to a single product in a narrow but distinct potential region: N_2. The pathway revealed here, i.e., reaction 9, was not discussed in our recent review on nitrogen cycle electrocatalysis.[7] However, as mentioned in the Introduction, very similar pathways have been observed in UHV surface science and in bacterial processes, the latter also at low (room) temperature. All these systems have the observation of a $^{14}N^{15}N$ product in common, with one N coming from a NH_x fragment and the other from a NO fragment. It is important to point out the significant advantage of this pathway over the more usual pathway for N_2 formation from $NO_3^-/NO_2^-/NO$ at low temperature. The more typical route involves a dimerization of NO to give a nitrous oxide intermediate (N_2O), which is subsequently reduced to N_2, as observed in nitrite and nitrate reduction on PdCu[62] and PtSn[63] electrodes. The classical biological nitrogen cycle also makes use of this route. The disadvantage of the "N_2O" pathway is that N_2O is a weakly coordinating molecule that easily escapes the catalytic site. Therefore, selectivity to N_2 is always far below 100%. On the other hand, the NH_x + NO route involves two strongly adsorbed intermediates and has the potential to generate 100% N_2.

CONCLUSIONS

Nitrite conversion to N_2 was studied at Pt(100) and related [(100) × (111)] and [(100) × (110)] stepped electrodes with in situ techniques (FTIRS, OLEMS). The insertion of increasingly denser defects of any symmetry caused a rapid decrease in the catalytic activity to N_2 formation: well-ordered Pt(100) was found to be the ideal surface for this reaction. Experimental evidence supported a mechanistic scheme based on a Langmuir–Hinshelwood recombination of two surface species which ultimately arise from nitrite (NO_{ads} and $NH_{x,ads}$) and which can be expected to coexist in the potential region of N_2 evolution. Our findings, highlighting the only known fully selective pathway leading from nitrite to N_2 for metals and biological systems, will help guide the design of practical catalysts, such as nanoparticles, with a view to applications in the field of wastewater treatment.

AUTHOR INFORMATION

Corresponding Author
m.duca@chem.leidenuniv.nl; m.koper@chem.leidenuniv.nl

ACKNOWLEDGMENT

We acknowledge partial financial support from the European Commission (through FP7 Initial Training Network "ELCAT", Grant Agreement No. 214936-2). M.T.M.K. acknowledges financial support from The Netherlands Organization for Scientific Research (NWO-Middelgroot) for the purchase and development of the online electrochemical mass spectrometer. J.M.F. acknowledges financial support from the Ministerio de Ciencia e Innovación (Spain) through Project CTQ2010-16271 (Feder).

REFERENCES

(1) Canfield, D. E.; Glazer, A. N.; Falkowski, P. G. *Science* **2010**, *330*, 192–196.
(2) Galloway, J. N.; Townsend, A. R.; Erisman, J. W.; Bekunda, M.; Cai, Z. C.; Freney, J. R.; Martinelli, L. A.; Seitzinger, S. P.; Sutton, M. A. *Science* **2008**, *320*, 889–892.
(3) Park, J. Y.; Yoo, Y. J. *Appl. Microbiol. Biotechnol.* **2009**, *82*, 415–429.
(4) Hiscock, K. M.; Lloyd, J. W.; Lerner, D. N. *Water Res.* **1991**, *25*, 1099–1111.
(5) Mateju, V.; Cizinska, S.; Krejci, J.; Janoch, T. *Enzyme Microb. Technol.* **1992**, *14*, 170–183.
(6) Fanning, J. C. *Coord. Chem. Rev.* **2000**, *199*, 159–179.
(7) Rosca, V.; Duca, M.; de Groot, M. T.; Koper, M. T. M. *Chem. Rev.* **2009**, *109*, 2209–2244.
(8) Gadde, R. R.; Bruckenstein, S. *J. Electroanal. Chem.* **1974**, *50*, 163–174.
(9) Nishimura, K.; Machida, K.; Enyo, M. *Electrochim. Acta* **1991**, *36*, 877–880.
(10) Ye, S.; Hattori, H.; Kita, H. *Ber. Bunsen-Ges. Phys. Chem.* **1992**, *96*, 1884–1886.
(11) Bae, I. T.; Barbour, R. L.; Scherson, D. A. *Anal. Chem.* **1997**, *69*, 249–252.
(12) da Cunha, M. C. P. M.; Nart, F. C. *Phys. Status Solidi A* **2001**, *187*, 25–32.
(13) Duca, M.; Cucarella, M. O.; Rodriguez, P.; Koper, M. T. M. *J. Am. Chem. Soc.* **2010**, *132*, 18042–18044.
(14) Duca, M.; Kavvadia, V.; Rodriguez, P.; Lai, S. C. S.; Hoogenboom, T.; Koper, M. T. M. *J. Electroanal. Chem.* **2010**, *649*, 59–68.
(15) Duca, M.; van der Klugt, B.; Hasnat, M. A.; Machida, M.; Koper, M. T. M. *J. Catal.* **2010**, *275*, 61–69.
(16) Nakata, K.; Doi, Y.; Kubota, S.; Shimazu, K. *J. Electroanal. Chem.* **2010**, *647*, 187–193.
(17) daCunha, M.; Weber, M.; Nart, F. C. *J. Electroanal. Chem.* **1996**, *414*, 163–170.
(18) Dima, G. E.; de Vooys, A. C. A.; Koper, M. T. M. *J. Electroanal. Chem.* **2003**, *554*, 15–23.
(19) Dima, G. E.; Beltramo, G. L.; Koper, M. T. M. *Electrochim. Acta* **2005**, *50*, 4318–4326.
(20) Taguchi, S.; Feliu, J. M. *Electrochim. Acta* **2007**, *52*, 6023–6033.
(21) Figueiredo, M. C.; Souza-Garcia, J.; Climent, V.; Feliu, J. M. *Electrochem. Commun.* **2009**, *11*, 1760–1763.
(22) Piao, S.; Kayama, Y.; Nakano, Y.; Nakata, K.; Yoshinaga, Y.; Shimazu, K. *J. Electroanal. Chem.* **2009**, *629*, 110–116.
(23) Koper, M. T. M. *Nanoscale* **2011**, *3*, 2054–2073.
(24) Rosca, V.; Koper, M. T. M. *Phys. Chem. Chem. Phys.* **2006**, *8*, 2513–2524.
(25) Vidal-Iglesias, F. J.; Garcia-Araez, N.; Montiel, V.; Feliu, J. M.; Aldaz, A. *Electrochem. Commun.* **2003**, *5*, 22–26.
(26) Vidal-Iglesias, F. J.; Solla-Gullon, J.; Rodriguez, P.; Herrero, E.; Montiel, V.; Feliu, J. M.; Aldaz, A. *Electrochem. Commun.* **2004**, *6*, 1080–1084.
(27) Vidal-Iglesias, F. J.; Solla-Gullon, J.; Montiel, V.; Feliu, J. M.; Aldaz, A. *J. Phys. Chem. B* **2005**, *109*, 12914–12919.
(28) Vidal-Iglesias, F. J.; Solla-Gullon, J.; Feliu, J. M.; Baltruschat, H.; Aldaz, A. *J. Electroanal. Chem.* **2006**, *588*, 331–338.
(29) Kartal, B.; Kuypers, M. M. M.; Lavik, G.; Schalk, J.; den Camp, H.; Jetten, M. S. M.; Strous, M. *Environ. Microbiol.* **2007**, *9*, 635–642.
(30) Kartal, B.; Kuenen, J. G.; van Loosdrecht, M. C. M. *Science* **2010**, *328*, 702–703.
(31) Hu, Y. H.; Griffiths, K.; Norton, P. R. *Surf. Sci.* **2009**, *603*, 1740–1750.
(32) Lombardo, S. J.; Esch, F.; Imbihl, R. *Surf. Sci.* **1992**, *271*, L367–L372.
(33) van Tol, M. F. H.; Siera, J.; Cobden, P. D.; Nieuwenhuys, B. E. *Surf. Sci.* **1992**, *274*, 63–81.
(34) Hallock, A. J.; Matthews, C. M.; Balzer, F.; Zare, R. N. *J. Phys. Chem. B* **2001**, *105*, 8725–8728.
(35) Lombardo, S. J.; Fink, T.; Imbihl, R. *J. Chem. Phys.* **1993**, *98*, 5526–5539.
(36) Tavares, P.; Pereira, A. S.; Moura, J. J. G.; Moura, I. *J. Inorg. Biochem.* **2006**, *100*, 2087–2100.
(37) Rafti, M.; Vicente, J. L. *Phys. Rev. E* **2007**, *75*, 7.
(38) Irurzun, I. M.; Mola, E. E.; Imbihl, R. *Chem. Phys.* **2006**, *323*, 295–303.
(39) Clavilier, J.; Armand, D.; Sun, S. G.; Petit, M. *J. Electroanal. Chem.* **1986**, *205*, 267–277.
(40) Rodes, A.; Zamakhchari, M. A.; El Achi, K.; Clavilier, J. *J. Electroanal. Chem.* **1991**, *305*, 115–129.
(41) Clavilier, J.; Faure, R.; Guinet, G.; Durand, R. *J. Electroanal. Chem.* **1980**, *107*, 205–209.
(42) Rosca, V.; Beltramo, G. L.; Koper, M. T. M. *Langmuir* **2005**, *21*, 1448–1456.
(43) Rodes, A.; Gomez, R.; Perez, J. M.; Feliu, J. M.; Aldaz, A. *Electrochim. Acta* **1996**, *41*, 729–745.
(44) Rodes, A.; Climent, V.; Orts, J. M.; Perez, J. M.; Aldaz, A. *Electrochim. Acta* **1998**, *44*, 1077–1090.
(45) de Vooys, A. C. A.; Koper, M. T. M.; van Santen, R. A.; van Veen, J. A. R. *J. Electroanal. Chem.* **2001**, *506*, 127–137.
(46) Wonders, A. H.; Housmans, T. H. M.; Rosca, V.; Koper, M. T. M. *J. Appl. Electrochem.* **2006**, *36*, 1215–1221.
(47) van der Vliet, D. F.; Koper, M. T. M. *Surf. Sci.* **2010**, *604*, 1912–1918.
(48) Al-Akl, A.; Attard, G. A.; Price, R.; Timothy, B. *J. Electroanal. Chem.* **1999**, *467*, 60–66.
(49) Sashikata, K.; Sugata, T.; Sugimasa, M.; Itaya, K. *Langmuir* **1998**, *14*, 2896–2902.
(50) Rodes, A.; Gomez, R.; Orts, J. M.; Feliu, J. M.; Perez, J. M.; Aldaz, A. *Langmuir* **1995**, *11*, 3549–3553.
(51) Nakamoto, K. *Infrared and Raman Spectra of Inorganic and Coordination Compounds*, 5th ed.; Wiley: New York, 1997.

(52) Yang, R. T.; Low, M. J. D. *Anal. Chem.* **1973**, *45*, 2014–2018.
(53) Bonner, O. D.; Curry, J. D. *Infrared Phys.* **1970**, *10*, 91–94.
(54) Rima, F. R.; Nakata, K.; Shimazu, K.; Osawa, M. *J. Phys. Chem. C* **2010**, *114*, 6011–6018.
(55) Rosca, V.; Koper, M. T. M. *J. Phys. Chem. B* **2005**, *109*, 16750–16759.
(56) Gomez, R.; Rodes, A.; Orts, J. M.; Feliu, J. M.; Perez, J. M. *Surf. Sci.* **1995**, *342*, L1104–L1110.
(57) Novell-Leruth, G.; Valcarcel, A.; Clotet, A.; Ricart, J. M.; Perez-Ramirez, J. *J. Phys. Chem. B* **2005**, *109*, 18061–18069.
(58) Offermans, W. K.; Jansen, A. P. J.; van Santen, R. A.; Novell-Leruth, G.; Ricart, J. M.; Perez-Ramirez, J. *J. Phys. Chem. C* **2007**, *111*, 17551–17557.
(59) Melius, C. F.; Binkley, J. S. *Symp. (Int.) Combust., [Proc.]* **1985**, *20*, 575–583.
(60) Wolf, M.; Yang, D. L.; Durant, J. L. *J. Phys. Chem. A* **1997**, *101*, 6243–6251.
(61) Abou-Rachid, H.; Pouchan, C.; Chaillet, M. *Chem. Phys.* **1984**, *90*, 243–255.
(62) de Vooys, A. C. A.; van Santen, R. A.; van Veen, J. A. R. *J. Mol. Catal. A* **2000**, *154*, 203–215.
(63) Yang, J.; Duca, M.; Schouten, K. J. P.; Koper, M. T. M. *J. Electroanal. Chem.* **2011**, in press; doi: 10.1016/j.jelechem.2011.03.015.